Cooperative Jahn–Teller effects in PrO_2

2008 J. Phys.: Condens. Matter 20 175218

(http://iopscience.iop.org/0953-8984/20/17/175218)

IOP PUBLISHING JOURNAL OF PHYSICS: CONDENSED MATTER

J. Phys.: Condens. Matter **20** (2008) 175218 (8pp) doi:10.1088/0953-8984/20/17/175218

Cooperative Jahn–Teller effects in PrO_2

D Ippolito[1], L Martinelli[1] and G Bevilacqua[2]

[1] CNISM and Dipartimento di Fisica 'E. Fermi', Via Buonarroti, 2, 56100 Pisa, Italy
[2] CNISM and Dipartimento di Ingegneria dell'Informazione, Università di Siena, Via Roma 56, 53100 Siena, Italy

E-mail: bevilacqua@unisi.it

Received 12 December 2007, in final form 6 March 2008
Published 7 April 2008
Online at stacks.iop.org/JPhysCM/20/175218

Abstract

A number of features recently observed experimentally in PrO_2, such as anomalies in the magnetic excitations spectrum, the reduction of the ordered magnetic moment below the Néel temperature, the distortion of the oxygen cage and the splitting of the ground state in the paramagnetic phase, are interpreted as consequences of electron–phonon coupling and cooperative effects. A coupling to phonons with trigonal symmetry is found appropriate to describe the experimental results. While a single center model can explain the reduction of the ordered magnetic moment and also the main features of the differential cross section, a cooperative model is necessary to interpret the observed distortion of the oxygen cage and the observed splitting of the ground state into two doublets in the paramagnetic phase.

1. Introduction

In recent years there has been a particular interest in the study of compounds containing localized 4f and 5f electrons, such as lanthanide dioxide PrO_2, [1–7] and the actinide dioxides UO_2 [8–13], NpO_2 [14–21] and PuO_2 [22, 23]. The most relevant experimental issues concerning PrO_2 are:

- At low temperature, PrO_2 (antiferromagnet with Néel point at $T_N = 13.5$ K) has an anomalously small magnetic moment [1, 4] when compared with the value expected for the ground electron-spin state in a cubic crystal field.
- The magnetic excitation spectra obtained at 10 K by inelastic neutron scattering by Boothroyd and co-workers [2] exhibit at low energy, besides two peaks separated by about 130 meV, a broad band (extending from 10 to 80 meV) centered at about 25–30 meV and a 160 meV shoulder.
- Neutron and x-ray diffraction measurements [5, 6] of the crystallographic and magnetic structure have revealed, below a temperature $T_D = (120 \pm 2)$ K, an internal distortion of the cubic oxygen cell surrounding the Pr^{4+} ion, confirmed by Webster *et al* [24] to be a distorted chiral structure.
- Measurements of the specific heat capacity [6] have shown that the Pr^{4+} ground state degeneracy is completely removed below T_N, while in the paramagnetic phase ($T_N < T < T_D$) the ground state is a doublet, consistent with a possible distortion of the crystal structure.
- Inelastic neutron scattering spectra made at increasing temperature [24] show that the central broad band is also present above T_N, but its maximum shifts toward lower energies when the temperature increases. A similar shift is also observed for the second peak.

From a theoretical point of view, recent first-principles studies of rare-earth dioxides [25] confirm the existence of a tetravalent ground state configuration or, in other words, that Pr^{4+} ions exist almost completely in a $4f^1$ configuration. Since the Pr^{4+} ground state is orbitally degenerate, a dynamical Jahn–Teller (JT) effect is expected. Actually, the broad continuum in the magnetic excitation spectrum as well the reduction of the ordered magnetic moment, when compared with the value expected for the ground electron-spin state in a cubic crystal field, have been interpreted as a manifestation of a dynamical JT effect [2, 7]. In fact JT coupling with phonon modes of proper symmetry can produce a number of levels having electronic and vibrational character [26, 27]. However, the distortion observed by neutron diffraction measurements cannot be interpreted without considering cooperative effects.

Since the pioneering works of Dunitz [29] and McClure [30] it is known that the interaction between JT active ions mediated by an elastic crystal lattice is a possible mechanism for structural phase transitions. In fact, at low temperature, the intercenter interaction (or cooperative interaction) can stabilize the JT distortion of each center, resulting in static distortion and the occurrence of level splitting becomes a characteristic feature of the symmetry lowering that accompanies

the phase transition. Cooperative JT effects [26, 35, 27] are seen in a variety of crystals, as described in a number of papers [31–34].

Very recently a model of the static and dynamical JT effect was proposed by Jensen [28] with the same purpose as ours, namely to give a unified description of different properties of PrO_2, but following a different approach in tackling dynamical JT effects and cooperative interactions. In [28] the observed distortion is considered to be a static JT effect, then the vibrational motion of oxygen ions produces a change of the CF Hamiltonian of the Pr ions and the JT term is considered to be induced by a local strain of t_2 symmetry. Moreover the antiferromagnetic phase is studied in detail, considering a superexchange interaction. So this approach leads to a different (and more complex) formalism; however, the results are similar to ours where a comparison is possible.

In this work, instead of the above approach, starting from an undistorted O_h symmetry we consider a dynamical JT coupling on each center and a cooperative interaction between neighboring centers induced by elastic interaction between symmetrized displacements. Then, always in the framework of a mean-field theory, we follow the decoupling procedure used by Feiner [36] and successively by Dunn [37]. This procedure, with respect to the phonon displaced operators approach [31, 32, 34], has the great advantage of retaining the vibronic effects associated with the local dynamics within a JT center, essential to reproduce the magnetic excitation spectra and the reduction of the ordered magnetic moment.

From the computational point of view, it is well known that the calculation of the eigenstates of a vibronic system requires handling matrices with a very large number of degrees of freedom. However, when linear JT coupling is considered, the matrices are in sparse form and then the Lanczos recursion procedure [38, 39] can be successfully used, provided that the initial state of the iterative procedure is chosen in a proper way [40, 7].

This paper is organized as follows. In section 2 we discuss the model Hamiltonian considered; in section 3 we show the calculation procedure and in section 4 we give the results obtained. Comments and conclusions are presented in section 5.

2. Model Hamiltonian

The electron states of Pr^{4+} ions interacting with the lattice displacements are well localized, therefore it is natural to consider a model Hamiltonian given by a sum of the local Hamiltonian H_i, describing the dynamics on the ith JT center, and the intercenter Hamiltonian $H_{j,i}$, describing the interaction between different centers. The total Hamiltonian is thus written [26] as

$$H = \sum_i H_i + \tfrac{1}{2} \sum_i \sum_{j \neq i} H_{j,i}. \tag{1}$$

In order to describe the single center Hamiltonian H_i let us discuss first the electron contribution H_e. PrO_2 has a fluorite structure type, where the Pr^{4+} ion is at the center of a cube whose vertices are occupied by eight O^{2-}. The

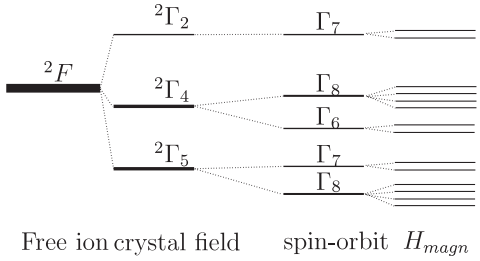

Figure 1. Level splitting of PrO_2 induced by the crystal field, spin–orbit interaction and magnetic field. The line thickness is proportional to the degeneracy of the level.

electron $4f^1$ configuration of the Pr^{4+} ion gives rise to a ground ^2F term 14-times degenerate including spin. The cubic crystalline field splits this term into states having the symmetry of the representations Γ_{5u}, Γ_{4u} and Γ_{2u} of the O_h group (Koster notation [41]), in increasing order of energy. The label u indicating the symmetry with respect to the inversion, is understood. The spin–orbit interaction $\lambda \mathbf{L} \cdot \mathbf{S}$ produces a further splitting of levels and, in the antiferromagnetic phase, a molecular exchange field interaction $H_{\text{magn}} = -\boldsymbol{\mu} \cdot \mathbf{H} = -g\mu_B \mathbf{H} \cdot \mathbf{J}$, where $\mathbf{H}$ is a local effective field acting on each magnetic dipole, completely removes the degeneracy [7]. In figure 1 we show a scheme of level splitting produced by these different interactions.

Recent neutron [24] and x-ray diffraction measurements [5, 6] suggest that a superposition of two 1-**k** structures oriented along mutually orthogonal directions is probably preferred. If we take the direction of the primary component of the local magnetic field as the z axis, the secondary one is oriented along the y axis, and defining $h_1 = g\mu_B H_z$ and $h_2 = g\mu_B H_y$, we can write $H_{\text{magn}} = h_1 J_z + h_2 J_y$. Therefore the electronic Hamiltonian includes the crystal field, spin–orbit and magnetic exchange interaction contributions:

$$H_e = H_{CF} + H_{SO} + H_{\text{magn}}. \tag{2}$$

Of course, the electronic Hamiltonian alone cannot reproduce the experimental issues, in particular the experimental cross section in the range 0–160 meV and the reduction of the ordered magnetic moment [2, 7].

Overcoming the Born–Oppenheimer approximation, the electronic states of the Pr ion are assumed to interact with phonon modes of proper symmetry localized around the Pr ion (JT ion) [44, 26].

In this specific system, the JT coupling involves states whose electronic part has Γ_4 or Γ_5 symmetry and consequently only the breathing, the tetragonal ϵ_g and the trigonal t_{2g} modes are active. The breathing mode produces only a line broadening and is neglected here; on the other hand the symmetry of the distortion indicates the prevalence of a trigonal mode. So we consider here a linear JT coupling with the same trigonal mode both on Γ_4 and on Γ_5 multiplets. In other words, we refer to a $(\Gamma_4 + \Gamma_5) \otimes t_2$ JT model. The vibrational Hamiltonian (H_v) and the electron–phonon Hamiltonian (H_{e-p}) are written, as usual, in the second

quantization notation:

$$H_{\rm v}(\Gamma_i) = \hbar\omega \left(a^{\dagger}_{yz}a_{yz} + a^{\dagger}_{xz}a_{xz} + a^{\dagger}_{xy}a_{xy} + \tfrac{3}{2}\right) P_{\Gamma_i}, \qquad (3)$$

$$H_{\rm e-p}(\Gamma_i) = \frac{\sqrt{3}}{2}\hbar\omega\sqrt{S(\Gamma_i)} \sum_{k=yz,xz,xy} (a^{\dagger}_k + a_k) D_k(\Gamma_i). \qquad (4)$$

Here Γ_i is for Γ_4 or Γ_5; P_{Γ_i} is the projector on the electron-spin eigenfunctions belonging to the Γ_i multiplet; yz, xz, xy indicate the rows of the t_{2g} mode; $S(\Gamma_i)$ is the Huang–Rhys factor or the JT energy in units of $\hbar\omega$; $D_k(\Gamma_i)$ are the Clebsch–Gordan coefficient matrices expressed on the basis of the electron functions belonging to the multiplet Γ_i; $H_{\rm v}$ and $H_{\rm e-p}$ are understood as multiplied by the identity in the spin space. In the following we refer to the JT Hamiltonian ($H_{\rm JT}$) as a sum of vibrational and electron–phonon parts: $H_{\rm JT} = H_{\rm v} + H_{\rm e-p}$, while the single center Hamiltonian is just the sum of the electronic and JT parts

$$H_i = H_{\rm e} + H_{\rm JT}. \qquad (5)$$

Let us now describe the intercenter Hamiltonian $H_{j,i}$. Since the $4f^1$ electron states of Pr^{4+} ion are well localized and the experiments [6] reveal that the Pr ions are not displaced from the equilibrium position, we have assumed that, in the inter-site Hamiltonian $H_{j,i}$, the contribution of the elastic interaction between symmetrized displacements predominates. Therefore we can write [26, 35, 27]

$$H_{j,i} = \mathbf{Q}^{\dagger}_i \mathbf{K}(i-j)\mathbf{Q}_j, \qquad (6)$$

where the vectors $\mathbf{Q}_i, \mathbf{Q}_j$ are a symmetrical combination of displacements of the oxygen ions surrounding the Pr ion in the site i and j; $\mathbf{K}(i-j)$ is a matrix whose components $K_{\Gamma\gamma\Gamma'\gamma'}(i-j)$ represent the strength of the interaction between a local mode $\Gamma\gamma$ on the center i and a local mode $\Gamma'\gamma'$ on the center j ($\Gamma\gamma$ indicates the row γ of the irreducible representation Γ).

The interdependence between the modes of centers i and j is decoupled in the framework of the mean-field approximation following the approach first introduced by Englman and Halperin [33] and used by Feiner and Dunn [36, 37] on prototype systems. This leads us to replace the total Hamiltonian H by a mean-field Hamiltonian $H^{\rm mf}$ which results in a sum of single-site terms $H^{\rm mf}_i$:

$$H^{\rm mf}_i = H_i + \sum_{\Gamma\gamma} f_{\Gamma\gamma}(i) Q_{\Gamma\gamma}(i).$$

Here H_i is the already discussed single center Hamiltonian and the second term, in the following called $H_{\rm coop}$, describes the intercenter interaction. In the cooperative term the quantity

$$f_{\Gamma\gamma}(i) = \sum_{j\neq i} \sum_{\Gamma'\gamma'} K_{\Gamma\gamma\Gamma'\gamma'}(i-j)\langle Q_{\Gamma'\gamma'}(j)\rangle \qquad (7)$$

represents the strength of the cooperative interaction on the center i and depends on the thermal average $\langle Q_{\Gamma'\gamma'}(j)\rangle$, ($\langle Q\rangle \equiv \sum_n \rho_n \langle\Psi_n|Q|\Psi_n\rangle$) so leading to a self-consistent procedure. Here $|\Psi_n\rangle$ are the vibronic eigenstates and ρ_n are the corresponding Boltzmann population factors.

In our system the JT active mode more appropriate to describe the experimental results is the trigonal or t_2 mode; then the cooperative contribution becomes:

$$H_{\rm coop} = \sqrt{\frac{\hbar}{\omega}} \sum_{k=yz,xz,xy} f_k \frac{1}{\sqrt{2}} \left(a^{\dagger}_k + a_k\right) \qquad (8)$$

where the strength coefficients f_{yz}, f_{zx}, f_{xy} can be better specified by taking into account the symmetry of the internal distortions (notice that we are using mass-weighted displacements [26]).

Recent experimental works [5, 6, 24] have shown that the magnetic structure and the structural distortions are related and that the neutron diffraction data are consistent with a distorted chiral structure, also confirmed by the theoretical work of Jensen [28].

In [43] it has been shown that, in the antiferromagnetic phase, it is possible to have a chiral distortion of the oxygen cage taking into account the experimental magnetic structure of Pr^{4+} ions with the primary component in the z direction and the secondary one in the y direction, then assuming a vibrational t_{2g} mode of the oxygen ions and considering that each O^{2-} ion belongs to four different cells. The sum of the contributions to the distortions from the different cells produces a chiral distortion and the effective displacements are a linear combination of symmetrized displacements Q_{yz} of the t_{2g} mode. We assume that the same distortion is found in the paramagnetic phase. The cooperative term has to produce the same type of distortion, then $\langle Q_{yz}(j)\rangle \neq 0$ and $\langle Q_{zx}(j)\rangle = \langle Q_{xy}(j)\rangle = 0$ also after the diagonalization of the full Hamiltonian. Then

$$f_{yz}(i) = \sum_{j\neq i} K_{yz,yz}(i-j)\langle Q_{yz}(j)\rangle \qquad (9)$$

alone contributes to the cooperative interaction. Performing the sum and taking into account only the nearest neighbors, the Hamiltonian (8) simplifies to

$$H_{\rm coop} = \frac{1}{\sqrt{2}} \frac{\sqrt{\hbar\omega}}{\omega} \left[K_{yz}\langle Q_{yz}\rangle \left(a^{\dagger}_{yz} + a_{yz}\right)\right] \qquad (10)$$

where the constant K_{yz} represents the strength of the cooperative interaction.

The mean-field Hamiltonian $H^{\rm mf}_i$ just discussed allows a quantitative connection between the properties of a JT center and the cooperative effects involving the same center. In other words, since the local dynamics of any center is explicitly included in $H^{\rm mf}_i$, it is possible to investigate the influence of such vibronic effects on the phase transitions as well as how the cooperative term influences the single center vibronic effects. In the single center Hamiltonian, however, we will consider only a one-mode vibronic model.

3. Calculation procedure

In the calculations we take as basis functions of our cooperative model the direct product of the 14 electron-spin function partners of the irreducible representations $\Gamma_8, \Gamma_7, \Gamma_6, \Gamma'_8, \Gamma'_7$

and of the vibrational states $|l, m, n\rangle$, where l, m, n are the occupation numbers for the partners of the t_2 phonon mode, in principle running from zero to infinity. It is well known that the number of phonons to achieve stable eigenstates increases with the strength of the JT coupling. In this way, the matrices involved in the calculations can quickly reach too large a rank to be diagonalized with traditional techniques. However, linear JT coupling leads to matrices in a sparse form, so allowing an efficient use of the Lanczos-recursion method [38, 39] with a proper number of over-recursions. An alternative approach to the diagonalization of the Lanczos matrices, particularly convenient when the number of recursions becomes too large, is constituted by the continued fraction expansion of the diagonal Green function matrix element $G_{00}(E)$, whose parameters are given by the coefficients (diagonal and off-diagonal) of the Lanczos chain [45]. The poles of the continued fraction give the eigenvalues of the vibronic system and their residua give the projected density of states which is immediately related to the optical spectra or to the differential cross section.

In order to determine the average internal displacements and the ordered magnetic moments, thermal averages of the corresponding operators have to be calculated:

$$\langle Q_{yz}\rangle = \frac{1}{\sqrt{2}}\sqrt{\frac{\hbar}{\omega}}\sum_n \rho_n \langle\Psi_n|\left(a^\dagger_{yz} + a_{yz}\right)|\Psi_n\rangle$$

$$\langle\mu_1\rangle = g_J \sum_n \rho_n \langle\Psi_n|J_z|\Psi_n\rangle\mu_B$$

$$\langle\mu_2\rangle = g_J \sum_n \rho_n \langle\Psi_n|J_y|\Psi_n\rangle\mu_B.$$

Let us now look at the differential cross section in the dipole approximation [46]:

$$\frac{d^2\sigma}{d\Omega d\omega}\frac{k_i}{k_f} = \left(\frac{\gamma e^2}{2m_e c^2} g_J\right)^2 F^2(\boldsymbol{\kappa}) \times \sum_{m,n}\rho_n \sum_{\alpha,\beta}(\delta_{\alpha,\beta} - \kappa_\alpha\kappa_\beta)$$
$$\times \langle\Psi_m|J^\dagger_\alpha|\Psi_n\rangle\langle\Psi_n|J_\beta|\Psi_m\rangle\delta(E_m - E_n - \tilde{\hbar\omega}). \qquad (11)$$

Here $|\Psi_n\rangle$ and $|\Psi_m\rangle$ are, respectively, the initial and final vibronic states involved in the transitions, J is the total angular momentum, $\boldsymbol{\kappa}$ is the scattering vector, $\mathbf{k}_i$ and $\mathbf{k}_f$ are initial and final neutron wavevectors, $F(\boldsymbol{\kappa})$ is the magnetic form factor and $\tilde{\hbar\omega}$ is the neutron energy transfer ($\tilde{\hbar\omega} = \frac{\hbar^2}{2m}(k_f^2 - k_i^2)$). Usually the experiments are performed at small $\boldsymbol{\kappa}$ where $F^2(\boldsymbol{\kappa}) \simeq 1$. So the main quantities to be calculated in the differential cross section (11) are the matrix elements $\langle\Psi_n|J_\alpha|\Psi_m\rangle$, which require knowledge of the vibronic functions $|\Psi_m\rangle$ and $|\Psi_n\rangle$. In principle, they could be evaluated through a two-pass Lanczos worked out for all the states of interest. However, as suggested in [7], it is enough to determine the vibronic starting state for the transition of interest. In fact, if we choose the initial state ϕ_0 of the Lanczos chain

$$|\phi_0\rangle = \frac{J_\alpha|\Psi_n\rangle}{\sqrt{\langle\Psi_n|J^2_\alpha|\Psi_n\rangle}}, \qquad (12)$$

the matrix element becomes

$$\langle\Psi_m|J_\alpha|\Psi_n\rangle = \langle\Psi_m|\phi_0\rangle\sqrt{\langle\Psi_n|J^2_\alpha|\Psi_n\rangle}. \qquad (13)$$

Then the differential cross section is immediately given by means of $|c_{m,0}|^2$, that is the projection modulus squared on the initial state of the Lanczos chain of the vibronic states of interest $|\Psi_m\rangle$ and their reconstruction is thus avoided.

4. Results

The diagonalization of the mean-field Hamiltonian H_i^{mf} has been carried out by means of the Lanczos recursion procedure with a suitable number of over-recursions so as to obtain reliable results and remove spurious eigenstates [47, 48]. When necessary, we have constructed the continued fraction expansion of the ground state Green's function $G_{00}(E)$, as described in the previous section.

The basis functions are allowed to span a vibronic space including up to a total number N of vibrational quanta chosen by looking at the stability of the eigenstates with respect to N. For the eigenvalues of interest we have required energy differences less than 0.5% going from N to $N + 1$. In practice, the maximum total number of phonons needed has been $N = 20$.

A number of independent parameters are involved in our model, so it is convenient to briefly comment on them. The crystal-field parameters F_4 and F_6 [49] mainly influence the energy separation among the multiplets Γ_5, Γ_4, Γ_2 and not the vibronic properties of the system, and their values have been taken equal to 228 meV and 140 meV, respectively, in such a way to have an energy separation of about 130 meV between the two main transitions of the magnetic excitation spectra at $T = 10$ K.

The value of the spin–orbit coupling constant λ, as usually given in the literature, has been assumed corresponding to the free ion value 100.5 meV.

The energy of the coupled phonon modes should be related to the lattice dynamics of PrO_2, but currently, to the best of our knowledge, neither experimental measurements nor theoretical calculations are available in the literature for the PrO_2 phonon branches. However, it is known that this energy determines the energy separations of the vibronic levels. Therefore the existence of a broad band centered at about 25–30 meV in the experimental spectra of the differential cross section [2] suggests a phonon energy mode of the same order. Here we have used $\hbar\omega = 30$ meV, as in a previous single center model [7].

We expect that the local effective magnetic exchange interaction mainly influences the ordered magnetic moments μ_1 and μ_2, and in fact the numerical simulations indicate that h_1 and h_2 play a secondary role on the neutron inelastic scattering spectrum, dominated by vibronic effects and CF effects.

Therefore it looks reasonable to take h_1 and h_2 in the same ratio as the measured magnetic moments. As a consequence, h_1 (or h_2) alone has to be taken as a free parameter, then phenomenologically estimated.

The strength of the JT coupling, here given in terms of the Huang–Rhys factor $S(\Gamma)$, directly influences the vibronic properties of the system and it is probably the most important parameter. It has been taken as a free parameter to be

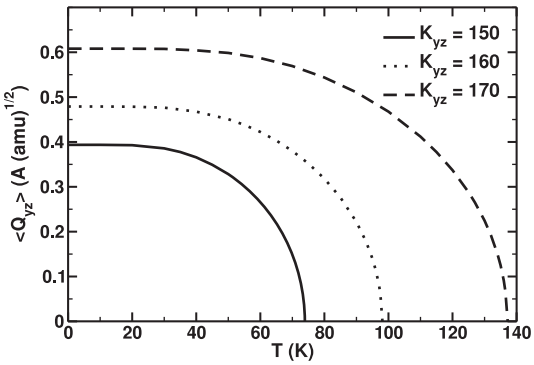

Figure 2. Mass-weighted $\langle Q_{yz}\rangle$ distortion as a function of the temperature for different values of K_{yz} (in meV (amu^{-1} Å^{-2})) with $S_{t_2}(\Gamma_4) = S_{t_2}(\Gamma_5) = 0.2$; $\hbar\omega_{t_2} = 30$ meV.

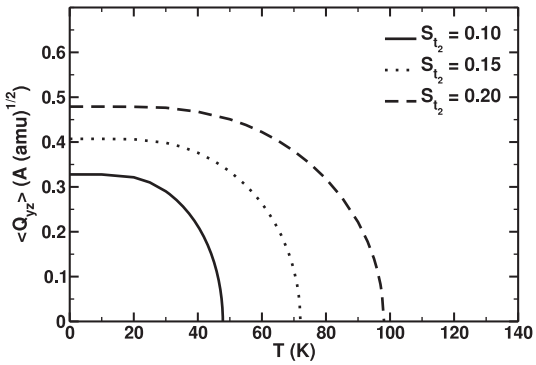

Figure 3. Mass-weighted $\langle Q_{yz}\rangle$ distortions as function of the temperature for different values of $S_{t_2} = S_{t_2}(\Gamma_4) = S_{t_2}(\Gamma_5)$ with $\hbar\omega_{t_2} = 30$ meV, $K_{yz} = 160$ meV (amu^{-1} Å^{-2}).

determined looking at the experimental neutron spectroscopic measurements.

The quantity K_{yz} characterizes the cooperative JT distortion and the phase transition temperature T_D.

In this work we are interested particularly in the cooperative effects; therefore, as a starting point, we have calculated the thermally averaged symmetrized displacements $\langle Q_{yz}\rangle$ as a function of the temperature for different values of K_{yz}, assuming at first equal coupling to the Γ_4 and Γ_5 multiplets, with a trial value $S_{t_2} = 0.2$ (a value used in a single center model). The results obtained are reported in figure 2, which exhibits the behavior of the thermally averaged displacement as a function of the temperature and calculated for different values of the cooperative constant K_{yz}. It can be seen that $\langle Q_{yz}(T)\rangle$ is almost constant for small values of T, then starts to decrease and goes rapidly to zero near to a certain temperature, interpreted as the transition temperature T_D from a distorted to an undistorted phase. When the cooperative constant K_{yz} increases, $\langle Q_{yz}(T)\rangle$ increases too and T_D becomes higher.

In order to study the influence of the electron–phonon coupling on the cooperative distortion $\langle Q_{yz}(T)\rangle$ we have performed calculations for different values of S_{t_2}, choosing $K_{yz} = 160$ meV (amu^{-1} Å^{-2}) with the other parameters as before. The results obtained are shown in figure 3. As can be seen, higher values of $\langle Q_{yz}(T)\rangle$ correspond to higher values of the vibronic coupling constant.

As can be seen from figures 2 and 3, stronger JT coupling at each center and stronger cooperative interaction lead to higher temperature for the phase transition. This is a second order phase transition and the temperature dependence of $\langle Q_{yz}\rangle$ in the neighborhood of the temperature T_D has been found to be $\langle Q_{yz}\rangle \approx \sqrt{T_D - T}$.

If now $S_{t_2}(\Gamma_4)$ is taken as different from $S_{t_2}(\Gamma_5)$, we obtain different values for the cooperative constants able to reproduce the structural phase transition at T = 120 K for different couples of $S_{t_2}(\Gamma_4)$ and $S_{t_2}(\Gamma_5)$. This situation is summarized in table 1 where we report the values of K_{yz} for which $\langle Q_{yz}(T)\rangle$ goes to zero for $T \simeq 120$ K and for different couples of $S_{t_2}(\Gamma_4)$ and of $S_{t_2}(\Gamma_5)$. It is evident that the cooperative JT distortion is favored by the increase in the electron–phonon coupling:

Table 1. Values of K_{yz} for which $\langle Q_{yz}(T)\rangle \simeq 0$ at $T \simeq 120$ K corresponding to different couples of $S_{t_2}(\Gamma_4)$ and $S_{t_2}(\Gamma_5)$.

	$S_{t_2}(\Gamma_5)$					
$S_{t_2}(\Gamma_4)$	0.0	0.2	0.4	0.6	0.8	1.0
0.0	—	204	195	187	179	171
0.2	185	166	156	148	141	134
0.4	173	147	139	132	126	120
0.6	149	133	126	120	115	110
0.8	136	123	116	111	106	102
1.0	125	113	108	103	99	95

increasing the strength of the JT coupling, the cooperative strength which restores the same T_D decreases.

Because there are many values of S_{t_2} that can lead to a structural phase transition at T = 120 K, in order to reduce them it is useful to look at the neutron scattering spectrum. It is well known that the strength of the JT coupling influences the vibronic functions and then the intensities of the transitions involved in the calculated differential cross section. The energies and the peak intensities of the vibronic levels obtained allow us to identify two main transitions shifted by about 130 meV, in the following called E_0 and E_1, and other transitions of different intensities in between due to the presence of many vibronic levels. A detailed analysis [43] of the behavior of the intensities of the elastic transition E_0 and the inelastic transitions E_1 and E_{int} (where E_{int} indicates the more pronounced intermediate transition), calculated as a function of the strength of the JT coupling on the electron states of Γ_5 and Γ_4 symmetries, suggests $0 < S_{t_2}(\Gamma_4) < 0.2$, $0.5 < S_{t_2}(\Gamma_5) < 1$ as convenient ranges to obtain a satisfactory agreement with the experimental spectra.

We have also studied to what extent the calculated spectrum depends on the cooperative parameter K_{yz} by looking at the behavior of the intensities of the same previously considered peaks as a function of the cooperative parameter K_{yz} and taking the Huang–Rhys factors at fixed values, for instance $S_{t_2}(\Gamma_4) = 0.1$ and $S_{t_2}(\Gamma_5) = 0.8$. The results obtained are shown in figure 4. As can be seen, the cooperative parameter influences mostly the intensity of the intermediate peak. The relative intensities of the calculated peaks can agree

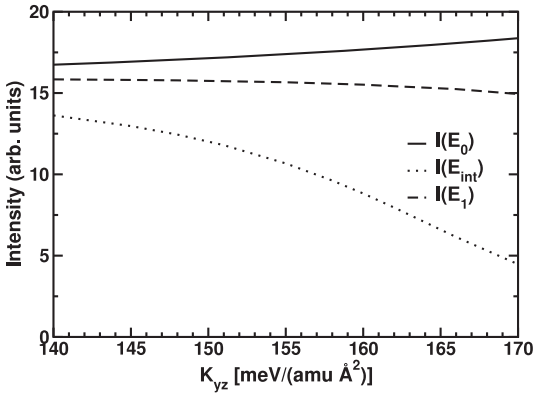

Figure 4. Intensities of the main peaks in the range 0–130 meV at $T = 10$ K as a function of K_{yz}; $S_{t_2}(\Gamma_4) = 0.1$ and $S_{t_2}(\Gamma_5) = 0.8$; $\hbar\omega_{t_2} = 30$ meV.

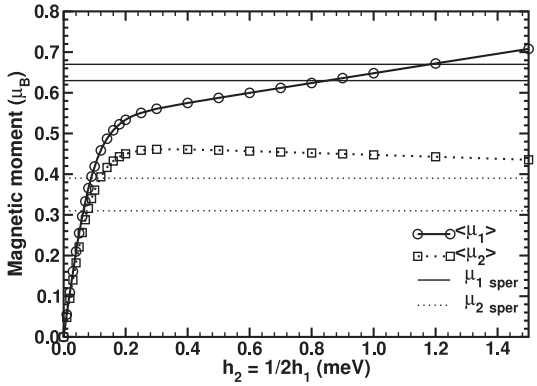

Figure 5. Cooperative model: behavior of $\langle\mu_1\rangle$, $\langle\mu_2\rangle$ at $T = 2$ K as a function of h_2, $\hbar\omega_{t_2} = 30$ meV, $S_{t_2}(\Gamma_4) = 0.1$, $S_{t_2}(\Gamma_5) = 0.8$, $K_{yz} = 160$ meV (amu^{-1} Å^{-2}).

with the experimental results for values of K_{yz} in the range $155 < K_{yz} < 165$ meV (amu^{-1} Å^{-2}), so in the following we will use $K_{yz} = 160$ meV (amu^{-1} Å^{-2}) for the calculation at $T < 10$ K. This value is consistent with the values given in table 1, but slightly higher (about 10%). In effect, with $S_{t_2}(\Gamma_4) = 0.1$ and $S_{t_2}(\Gamma_5) = 0.8$, it is the value $K_{yz} = 144$ meV (amu^{-1} Å^{-2}) that restores $T_D = 120$ K. Probably this slight dependence of K_{yz} on the temperature could indicate the presence of some minor effects not considered in our model, as, for instance, higher order terms in the JT coupling.

Let us now consider the ordered magnetic moment in the antiferromagnetic phase. The measurements of Kern [1] in 1984 gave $\mu = (0.6 \pm 0.1)\ \mu_B$; afterwards Gardiner and co-workers [4] obtained $\mu = (0.68 \pm 0.07)\ \mu_B$ in crystals and $\mu = (0.572 \pm 0.012)\ \mu_B$ in powders; more recently Gardiner *et al* [5] have measured two mutually orthogonal components of the magnetic moment at $T = 2$ K: $\mu_1 = (0.65 \pm 0.02)\mu_B$ and $\mu_2 = (0.35 \pm 0.04)\mu_B$.

In our calculations we have considered the magnetic structure suggested in the more recent experiments [5], and we have chosen $h_1 = 2h_2$, consistent with the experimental ratio of μ_1 and μ_2. Then we studied the behavior of the ordered magnetic moments at $T = 2$ K, taking $K_{yz} = 160$ meV (amu^{-1} Å^{-2}) and all the other parameters fixed as in the previous calculations. In figure 5 we show the results obtained as a function of h_2. The experimental values are considered in a band as large as the estimated uncertainties. For $0.8 < h_2 < 1.2$ meV, the calculated $\langle\mu_1\rangle$ agrees well with the experimental value, instead $\langle\mu_2\rangle$ remains higher by about 25%.

In the upper part of figure 6 we show the differential cross section calculated at $T = 10$ K (continuous line) with $S_{t_2}(\Gamma_4) = 0.1$, $S_{t_2}(\Gamma_5) = 0.8$, $h_2 = 0.8$ meV and $K_{yz} = 160$ meV (amu^{-1} Å^{-2}).

It is worth noting that even if the strength of the magnetic exchange interaction does not influence the overall structure of the magnetic excitation spectra, when h increases the shift of the main peak with respect to the zero energy increases too. Choosing $h_2 = 0.8$ meV (as in figure 6), the main peak results

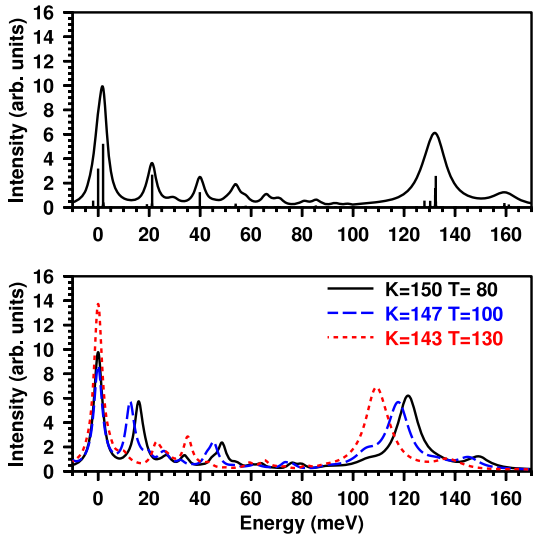

Figure 6. Upper part: differential cross section at $T = 10$ K. Lower part (color): differential cross section at $T = 80$, 100 and 130 K. The parameters used are given in the text.

(This figure is in colour only in the electronic version)

are centered at about 3 meV as experimentally observed [2]. In the intermediate region, in between 20–80 meV far from the main peak, there are several transitions with decreasing intensity moving towards higher energies; other transitions are found at about 160 meV. Of course, as shown elsewhere [7], a multimode JT model could produce a yet larger number of levels in the intermediate region, so improving the agreement with the experimental results.

Next we calculated the magnetic excitation spectrum at $T > T_N$. The spectrum at $T = 20$ K (not shown here) is very similar to that at $T = 10$ K, except that the first peak is now centered on zero energy. The spectra at $T = 80$, 100 and 130 K are shown in the lower part of figure 6. All the parameters are taken equal as before, except that K_{yz} has been chosen about equal to 150, 147, 143 meV (amu^{-1} Å^{-2}), respectively assuming a linear decreasing of K_{yz} when the temperature increases and taking into account that K_{yz} has to be chosen

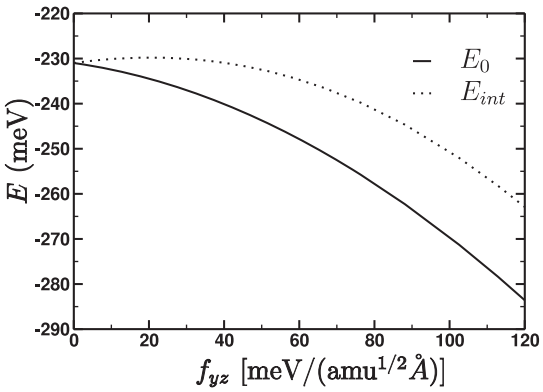

Figure 7. Splitting of the ground state at $T = 20$ K. All the parameters are the same as previously used at $T = 10$ K. The f_{yz} values corresponding to the K_{yz} chosen in figures 5 and 6 are: $f_{yz} \approx 120$ in figures 5 and 6 (upper side); $f_{yz} \approx 80, 56, 0$ in the lower side of figure 6.

equal to 144 meV (amu^{-1} Å^{-2}) in order to obtain the transition temperature at $T = 120$ K.

Some significant differences can be noticed from the upper and lower parts of the figure: in the lower part the first peak is centered on zero energy, the second one is shifted towards lower energies, as well as those at about 130 and 160 meV; moreover at $T > T_D$ the second peak disappears and the intermediate transitions are very similar to those obtained in a single center model [7]. This behavior agrees with the more recent experimental spectra of Webster *et al* [24], even if the shift calculated is more pronounced than the experimental one. The role of the cooperative interaction in the intermediate band of the magnetic excitation spectra at $T < T_D$ is so evident: leading to a static distortion it provides a mechanism which lowers the symmetry of the system and produces a splitting of the four-degenerate ground state observed experimentally [5] and confirmed by our simulations (see also figure 7 where the splitting into double degenerate states E_0, E_{int} is shown as a function of the cooperative strength). As a consequence, at $T < T_D$ a relevant contribution to the central band is due just to the transitions towards the split level.

5. Conclusions

A microscopic model including the crystal field, the magnetic exchange interaction and a polycenter dynamical JT coupling has been proposed to interpret a number of experimental facts such as anomalies in the neutron spectrum of PrO_2, the reduction of the ordered magnetic moment for $T < T_N$, the distortion of the oxygen cage and the structural phase transition.

While a single center model of dynamical JT coupling with phonons of trigonal symmetry could explain the reduction of the ordered magnetic moment and also the main features of the differential cross section, a cooperative interaction is necessary to interpret the observed distortion at $T < 120$ K and the splitting of the ground state into two doublets in the paramagnetic phase [5].

The Lanczos recursion procedure, in connection with the Green function formalism, has been followed and adapted to calculate with high precision the vibronic levels of Pr^{4+} ions on PrO_2. A suitable choice for the initial state of the Lanczos procedure has allowed easy calculation of the differential cross section for comparison with neutron spectroscopy measurements. The ordered magnetic moment too has been directly evaluated, as well as the distortion of the oxygen cage and the temperature effects on the inelastic neutron spectra.

The strength of the interactions taken into account have been phenomenologically determined to achieve agreement with the experimental results. Even if the model presents some limitations (single mode JT coupling, magnetic exchange interaction treated through a free parameter) it provides a simple means for evaluating the main characteristic effects of a dynamic cooperative interaction, gives a satisfactory explanation for a number of experimental facts and supplies a reasonable range of values for the strength of the interaction involved, so representing a starting point for the next interpretative models.

References

[1] Kern S, Loong C-K, Faber J and Lander G H 1984 *Solid State Commun.* **49** 295
Kern S, Loong C-K and Lander G H 1985 *Phys. Rev.* B **32** 3051
Kern S, Trouw F, Loong C-K and Lander G H 1990 *J. Appl. Phys.* **67** 4830
[2] Boothroyd A T, Gardiner C H, Lister S J S, Santini P, Rainford B D, Noailles L D, Currie D B, Eccleston R S and Bewley R I 2001 *Phys. Rev. Lett.* **86** 2082
[3] Dabrowski J, Zavodinsky V and Fleszar A 2001 *Microelectron. Reliab.* **41** 1093
[4] Gardiner C H, Boothroyd A T, Lister S J S, McKelvy M J, Hull S and Larsen B H 2002 *Appl. Phys.* A **74** S1773
[5] Gardiner C H, Boothroyd A T, Pattison P, McKelvy M J, McIntyre G J and Lister S J S 2004 *Phys. Rev.* B **70** 024415
[6] Gardiner C H, Boothroyd A T, McKelvy M J, McIntyre G J and Prokes K 2004 *Phys. Rev.* B **70** 024416
[7] Bevilacqua G, Ippolito D and Martinelli L 2004 *Phys. Rev.* B **69** 155208
[8] Amoretti G, Blaise A, Caciuffo R, Fournier J M, Hutchings M T, Osborn R and Taylor A D 1989 *Phys. Rev.* B **40** 1856
[9] Caciuffo R, Amoretti G, Santini P, Lander G H, Kulda J and Du Plessis P de V 1999 *Phys. Rev.* B **59** 13892
[10] Ikushima K, Tsutsui S, Haga Y, Yasuoka H, Walstedt R E, Masaki N M, Nakamura A, Nasu S and Onuki Y 2001 *Phys. Rev.* B **63** 104404
[11] Kudin K N, Scuseria G E and Martin R L 2002 *Phys. Rev. Lett.* **26** 266402
[12] Laskowski R, Madsen G K H, Blaha P and Schwarz K 2004 *Phys. Rev.* B **69** 140408
[13] Ippolito D, Martinelli L and Bevilacqua G 2005 *Phys. Rev.* B **71** 064419
[14] Amoretti G, Blaise A, Caciuffo R, Di Cola D, Fournier J M, Hutchings M, Lander G H, Osborn R, Severing A and Taylor A D 1992 *J. Phys.: Condens. Matter* **4** 3459
[15] Mannix D, Lander G H, Rebizant J, Caciuffo R, Bernoheft N, Lidströ E and Vettier C 1999 *Phys. Rev.* B **60** 15187
[16] Paixao J A, Detlefs C, Longfield M J, Caciuffo R, Santini P, Bernoheft N, Rebizant J and Lander G H 2002 *Phys. Rev. Lett.* **89** 187202

[17] Lovesey S W, Blacar E, Detlefs C, Van Der Laan G, Silvia D S and Staub U 2003 *J. Phys.: Condens. Matter* **6** 383
[18] Tokunaga Y, Homma Y, Kambe S, Aoki D, Sakai H, Yamamoto E, Nakamura A, Shiokawa Y, Walsted R E and Yasuoka H 2005 *Phys. Rev. Lett.* **94**
[19] Magnani N, Santini P, Amoretti G, Caciuffo R, Javorsky P, Wastin F, Rebizant J and Lander G H 2005 *Physica* B **359** 1087
[20] Nagao T and Igarashi J 2005 *Phys. Rev.* B **72** 4421
[21] Kubo K and Hotta T 2005 *Phys. Rev.* B **72** 132411
[22] Kern S, Robinson R A, Nakotte H, Lander G H, Cort B, Watson P and Vigil F A 1999 *Phys. Rev.* B **59** 104
[23] Colarieti Tosti M, Eriksson O, Nordstrom L, Wills J and Brooks M S S 2002 *Phys. Rev.* B **65** 195102
[24] Webster C H, Helme L M, Boothroyd A T, McMorrow D F, Wilkins S B, Detlefs C, Detlefs B, Bewley R I and McKelvy M J 2007 *Phys. Rev.* B **76** 134419
[25] Petit L, Svane A, Szotek Z and Temmerman W M 2005 *Phys. Rev.* B **72** 205118
[26] Bersuker I B and Polinger V Z 1989 *Vibronic Interactions in Molecules and Crystals* (*Springer Series in Chemical Physics*) (Berlin: Springer)
[27] Bersuker I B 2006 *The Jahn–Teller Effect* (Cambridge: Cambridge University Press)
[28] Jensen J 2007 *Phys. Rev.* B **76** 144428
[29] Dunitz J D and Orgel L E 1957 *J. Phys. Chem. Solids* **3** 20
[30] McClure D S 1957 *J. Phys. Chem. Solids* **3** 311
[31] Kanamori J 1960 *J. Appl. Phys.* **38** 14S
[32] Elliott R J, Ghering G A, Malozemoff A P, Smith S R P, Staude W S and Tyte R N 1971 *J. Phys. C: Solid State Phys.* **4** L179
Elliott R J, Harley R T, Hayes W and Smith S R P 1972 *Proc. R. Soc.* A **238** 217
[33] Englman R and Halperin B 1970 *Phys. Rev.* B **2** 75
Halperin B and Englman R 1971 *Phys. Rev.* B **3** 1698
[34] Gehring G A and Gehring K A 1975 *Rep. Prog. Phys.* **38** 1
[35] Kaplan M D and Vekhter B G 1995 Copperative phenomena in Jahn–Teller crystals *Modern Inorganic Chemistry* (New York: Plenum)
[36] Feiner L F 1982 *J. Phys. C: Solid State Phys.* **15** 1495
[37] Dunn J L 2004 *Phys. Rev.* B **69** 064303
[38] Lanczos C 1950 *J. Res. Natl Bur. Stand.* **45** 255
Lanczos C 1952 *J. Res. Natl Bur. Stand.* **49** 33
Lanczos C 1956 *Applied Analysis* (Englewood Cliffs, NJ: Prentice-Hall)
[39] Haydock R, Heine V and Kelly M J 1972 *J. Phys. C: Solid State Phys.* **5** 2845
Haydock R, Heine V and Kelly M J 1975 *J. Phys. C: Solid State Phys.* **8** 2591
see also Bullet D W, Haydock R and Kelly M J 1980 *Solid State Physics* vol 35 ed H Erhenreich, F Seitz and D Turnbull (New York: Academic)
[40] Martinelli L, Passaro M and Pastori Parravicini G 1989 *Phys. Rev.* B **39** 13343
[41] Koster G F, Dimmock J O, Wheeler R G and Statz H 1963 *Properties of the Thirty-Two Point Groups* (Cambridge, MA: MIT University Press)
[42] Tindemans-van Eijndhoven J C M and Kroese C J 1975 *J. Phys. C: Solid State Phys.* **8** 3963
[43] Ippolito D 2006 Jahn–Teller effect on rare earth dioxides *PhD Thesis* Department of Physics, University of Pisa
[44] Sturge M D 1967 *Solid State Physics* vol 20, ed F Seitz, D Turnbull and H Ehrenreich (New York: Academic) p 92
[45] Grosso G and Pastori Parravicini G 1985 *Adv. Chem. Phys.* **62** 81
Grosso G and Pastori Parravicini G 1985 *Adv. Chem. Phys.* **62** 133
[46] Marshall W and Lovesey S W 1971 *Theory of Thermal Neutron Scattering* (Oxford: Oxford University Press)
Lovesey S W 1984 *Theory of Thermal Neutron Scattering from Condensed Matter* (Oxford: Oxford University Press)
[47] Cullum J C and Willoughby R A 1985 *Lanczsos Algorithms for Large Symmetric Eigenvalue Computations* vols I and II (Boston, MA: Birkhauser)
[48] Martinelli L, Bevilacqua G, Rivera-Iratchet J, de Orue M A, Mualin O, Vogel E E and Cartes J 2000 *Phys. Rev.* B **62** 10873
[49] Bersuker I B 1996 *Electronic Structures and Properties of Transition Metal Compounds* (New York: Wiley Interscience)